WCDMA STTD Performance Analysis with Transmitter Location Optimization in Indoor Systems Using Ray-tracing Technique

***Kyung K. Bae, *Jing Jiang, *William H. Tranter, *C. R. Anderson and ***T. S. Rappaport**
****Jian He, **Alex Verstak, **L. T. Watson, **N. Ramakrishnan, and **C. A. Shaffer**

*Mobile and Portable Radio Research Group (MPRG)
432 Durham Hall, Mail Stop 0350
Bradley Dept. of Elec. & Comp. Engineering, Virginia Polytechnic Institute and State University
Blacksburg, VA, USA, 24061, Phone: (540) 231-2967, FAX: (540) 231-2968, E-mail: kbae@vt.edu

** Department of Computer Science
Virginia Polytechnic Institute and State University, Blacksburg, VA, USA, 24061

***Department of Electrical and Computer Engineering, University of Texas, Austin, TX, 78712-1084

Abstract – *This paper presents the performance of space-time block coding based transmit diversity (STTD) in WCDMA on correlated fading channels and on unbalanced transmitted power. Then, based on the performance, transmitter location optimization in indoor environments is considered. Results indicate that the effective diversity order is retained even when high cross correlation exists and power imbalance exists between signals from different antennas. Also, a global optimization algorithm with the help of a ray tracer can find transmitter locations which are optimal (global optimum) in the sense of power coverage or overall BER in the area of interest.*

1. Introduction

As the demand for different types of services such as voice, data, and video increases, more reliable communication techniques are required in order to accommodate various types of traffic such as low data rate voice and high data rate data packets. Especially in the case of data communications, the more reliable the links between transmitters and receivers, the less resources will be consumed in retransmitting data. One way of increasing link reliability is to use diversity techniques. STTD, which has been accepted as an open loop transmit diversity in WCDMA, has shown diversity gains on even correlated and power-unbalanced channels. In this paper, we investigate STTD performance and automatic base-station placements at optimal sites (optimal in the sense that the overall BER on the planning area is minimized), and the impact of STTD on indoor WCDMA system design - transmitter location optimization.

2. Space-time Transmit Diversity (STTD)

Space-time transmit diversity is an open loop transmit diversity based on the space-time block code [1] proposed by Alamouti. Space-time transmit diversity improves the signal quality at the receiver by introducing space diversity through simple signal processing across two transmit antennas. The scheme uses two transmitter antennas and one receiver antenna. Let s_0 and s_1 be complex signals representing the in-phase and quadrature component in QPSK modulation. Signals s_0 and s_1 are simultaneously transmitted from antenna 1 and antenna 2 respectively during one symbol period, while $-s_1^*$ and s_0^* are simultaneously transmitted from antenna 1 and antenna 2, respectively, during the next symbol period. Suppose there are L resolvable multipaths, then the received signals on the j[th] path at time t and $t+T$ are given by

$$r_0^j = r^j(t) = h_0^j s_0 + h_1^j s_1 + n_0 \qquad (1)$$
$$r_1^j = r^j(t+T) = -h_0^j s_1^* + h_1^j s_0^* + n_1$$

where h_i^j , $i=0,1$, $j=1,...,L$ are the channel coefficients on the j[th] multipath between the transmitter antenna i , $i=0,1$ and the receiver antenna, n_0 and n_1 are the additive white Gaussian noises, and * denotes the complex conjugate. The channel coefficients at time t and $t+T$ are modeled by a complex multiplicative distortion h_i^j , $i=0,1$, $j=1,...,L$ assuming that fading is constant across two consecutive symbols [1]. The combining scheme for STTD at the receiver produces the following soft estimates for the symbols s_0 and s_1 on the jth multipath respectively:

$$\tilde{s}_0^j = \tilde{h}_0^{j*} r_0 + \tilde{h}_1^j r_1^* \qquad (2)$$
$$\tilde{s}_1^j = \tilde{h}_1^{j*} r_0 - \tilde{h}_0^j r_1^*$$

where $\tilde{h}_i^j$ represents the channel coefficient estimate of h_i^j. The soft estimates from all the resolvable multipath components can now be combined. A conventional RAKE receiver combines soft estimates from all the multipaths. The final soft estimates $\tilde{s}_0$ and $\tilde{s}_1$ after

space-time block decoding and Rake combining can be expressed respectively

$$\tilde{s}_0 = \sum_{j=1}^{L} \tilde{s}_0^j = \sum_{j=1}^{L} \left(\tilde{h}_0^{j*} r_0 + \tilde{h}_1^j r_1^* \right) \qquad (3)$$

$$\tilde{s}_1 = \sum_{j=1}^{L} \tilde{s}_1^j = \sum_{j=1}^{L} \left(\tilde{h}_1^{j*} r_0 - \tilde{h}_0^j r_1^* \right)$$

Therefore, the total diversity order for each of the symbols s_0 and s_1 is 2L, which is twice the diversity order of the system without space diversity.

For a system with n_T transmit antennas and 1 receive antenna, assuming flat fading, the average symbol error probability is bounded by [2]

$$\overline{P}_e \le \sum_{i=1}^{n_T} a_i \left[1 - \frac{1}{\sqrt{1 + \frac{2}{\lambda_i \gamma_{eq}}}} \right], \text{where } a_i = \frac{\lambda_i^{(n_T-1)}}{\prod_{\substack{i=1 \\ i \ne m}}^{n_T} (\lambda_i - \lambda_m)} \qquad (4)$$

where λ_i represents the eigenvalues of the covariance matrix $\Sigma = E[(\Omega - \bar{\Omega})(\Omega - \bar{\Omega})^\dagger]$, $\Omega = [h_1, h_2, ..., h_{n_T}]^T$, the h_i's are complex fade channel coefficients which are complex Gaussian random process for Rayleigh fading, $\bar{\Omega} = E[\Omega]$, and † denotes the Hermitian operation. $\gamma_{eq} = [2SNR \sin^2(\pi / M)]/[rn_T]$ is the equivalent SNR, taking into account the M-ary signaling, orthogonal design rate r, and the number of elements at the transmitter. For a system with QPSK modulation, $n_T = 2$, and 1 receive antenna, (4) becomes [2]

$$\overline{P}_e \le \frac{1}{\lambda_1 - \lambda_2} \left[\lambda_1 \left(1 - \frac{1}{\sqrt{1 + (\lambda_1 SNR/2)^{-1}}} \right) - \lambda_2 \left(1 - \frac{1}{\sqrt{1 + (\lambda_2 SNR/2)^{-1}}} \right) \right] \qquad (5)$$

Equation (5) give tight bound on the performance of STTD on correlated flat fading channels.

3. Parallel Ray Tracer

Received impulse responses are approximated with a 3D ray tracing propagation model that is based on geometrical optics. Electromagnetic waves are modeled as rays that are traced through reflections and transmissions through walls. Beams are shot from geodesic domes drawn around transmitters. Essentially, the spherical wavefront is triangulated and the 3D sphere is split into pyramidal beams. All such beams are disjoint and have nearly the same shape and angular separation [3]. Only the central ray of each beam is traced to identify reflection locations. However, the whole beam is used for ray-receiver intersection tests. Once an intersection with a receiver location is detected, a ray will be traced back from the receiver to the transmitter through the sequence of reflections and transmissions (penetrations) encountered by the beam. Neither diffraction nor scattering are modeled for computational complexity reasons, although these phenomena may play an important role in propagation [4]. Octree space partitioning [5] and image parallelism with dynamic scheduling [6] are used to reduce simulation run time.

Although material parameters and incidence angles affect losses in a wireless channel, a constant 6 dB reflection loss (same as in [7]) and a constant 4.6 dB transmission (penetration) loss (the loss for plaster board in [8]) are assumed. The power contribution of each ray, in dBW, is calculated according to the model developed in [3]:

$$P_j = P(d_0) - 20\log_{10}(d/\lambda) - nL_r - mL_t \qquad (6)$$

where P_j is the power of the j-th ray, d is the total distance traveled by the ray, $P(d_0)$ is the transmitter power at a reference distance d_0 from the transmitter, n and m are the numbers of reflections and transmissions, L_r = 6 dB and L_t = 4.6 dB are reflection and transmission losses, and λ is the wavelength.

The ray tracer has been validated and calibrated with a series of measurements in the corridor of the fourth floor of Durham Hall, Virginia Tech. An ultrawideband sliding correlator channel sounder operating at 2.5 GHz with omnidirectional antennas was used to record power delay profiles (PDPs) at six separate locations. The sliding correlator utilized an 11-bit, 400 MHz pseudo-noise spreading code for a time domain multipath resolution of 2.5 nanoseconds and a dynamic range of 30 dB. Simulated power delay profiles were post-processed and compared to the measured ones location by location.

The received E-field envelope of ray j (in V/m) that arrived at time t_j is $E_j = \sqrt{\eta 10^{0.1P_j}}$, where P_j is the output of the ray tracer (in dBW) and $\eta = 120\pi\ \Omega$ is the impedance of free space [4]. To account for antenna directivity, an omnidirectional antenna pattern must be applied to all E_js. The electric field that would be registered at time t_j by a hypothetical measurement system with infinite bandwidth resolution is

$$E_j' = E_j G_t G_r \cos\Theta_t \cos\Theta_r \ , \qquad (7)$$

where Θ_t and Θ_r are ray transmission and reception elevation angles relative to the horizon, and G_t and G_r are transmitter and receiver antenna gains, respectively. Since the measurement system had 2.5 ns time domain resolution, ray tracer outputs are convolved with a Gaussian filter and sampled at uniform time interval of

width δ. The measurement system output samples with $\delta = 1\ ns$ while WCDMA simulation used chip time $\delta \approx 260\ ns$. The measured electric field E_k^m of bin k centered at time $k\delta$ is

$$E_k^m = C\sum_{j=1}^{Q} E_j' e^{i\phi_j} \int_{t_j - k\delta - \delta/2}^{t_j - k\delta + \delta/2} e^{-\tau^2/(2\sigma^2)} d\tau, \qquad (8)$$

where Q is the number of rays from ray tracer, σ is the half-width of the Gaussian pulse (1.25 ns for measurements), and C is a scale factor that fits this generic equation to a particular system. Since most of the energy in the Gaussian pulse should fall into one time interval of δ,

$$C\int_{-\delta/2}^{\delta/2} e^{-\tau^2/(2\sigma^2)} d\tau = 1 \qquad (9)$$

Hence, every time bin registers a weighted average of the energies of all predicted rays, where the weight decreases exponentially as the time difference of the ray and the bin increases. Phase angles ϕ_j in $e^{i\phi_j}$ were determined from transmitter wavelength λ, total ray path length d_j, and the number of reflections n (a 180 degree phase shift per reflection was assumed). Finally, $P_k^m = |E_k^m|^2 / \eta$ gives the measured power of bin k, in watts.

Figure 1 shows measurements and predictions for one location with relatively strong multipath. As can be seen from the graph, the predictions are within 3~5 dB of the measurements, which is similar to the results achieved by earlier research [3]. The difference can be explained by device positioning errors (devices were positioned with $\pm 3\ cm$ precision, which is crude given that the wavelength was 12cm) and imprecise modeling of reflections. Additionally, small multipath components were missed by the ray tracer. These components are probably due to scattering and diffraction, which were not simulated. Geodesic tessellation frequency was 300 for calibration.

4. Optimization

The objective of optimization is to maximize the average performance over m receiver locations given that there are n transmitters in an indoor environment. The variables are the transmitter coordinates

$$X = (x_1, y_1, z_1, x_2, y_2, z_2, \ldots, x_n, y_n, z_n),$$

where all $z_j = z_0$ are fixed, a reasonable assumption for indoor environments. Let transmitter (k,i), located at (x_k, y_k, z_0), $1 \le k \le n$, generate the highest power level $P_{ki}(x_k, y_k, z_0) \ge P_{ji}(x_j, y_j, z_0)$, $1 \le j \le n$, at the receiver location i, $1 \le i \le m$. The objective function is the average shortfall of the estimated performance metric from the given threshold T, given by

$$f(X) = \begin{cases} \dfrac{1}{m}\sum_{i=1}^{m} (T - p_{ki})_+, & coverage \\ \dfrac{1}{m}\sum_{i=1}^{m} (p_{ki} - T)_+, & BER \end{cases} \qquad (10)$$

where p_{ki} is the performance metric of transmitter (k,i) evaluated at the i^{th} receiver location. For power coverage optimization, p_{ki} is $P_{ki}(x_k, y_k, z_0)$ and $(T - p_{ki})_+$ is the penalty for a lower power level than a target power. For BER optimization, p_{ki} is $\log_{10}(BER_{ki})$ and $(p_{ki} - T)_+$ is the penalty for higher bit error rate than a target BER.

An efficient pattern search algorithm - DIRECT (DIviding RECTangles) proposed by Jones, Perttunen, and Stuckman (1993) - has been used to optimize the location of transmitter in indoor environments [9].

5. Simulation Results and Conclusion

S^{4}W (Site-Specific System Simulator), an indoor wireless system design tool, has been developed for link-level simulations and transmitter location optimizations. The S^{4}W consists of five modules, which are a link-level WCDMA simulator, a 3D ray tracer, an optimizer, an execution manager, and a database. Figure 2 shows the block diagram of S^{4}W indoor wireless system design tool. For a given indoor environment, the ray-tracer predicts channel characteristics, and then the link-level WCDMA simulator performs simulations based on site-specific channel characteristics. Optimizer optimizes transmitter locations according to two different criteria mentioned in section 4. All simulations for ray-tracer, WCDMA link-level simulator, and optimizer have been parallelized.

Figure 3 shows that the diversity gain achieved by STTD is still retained for cross-correlation coefficients between channels as high as 0.7. In Figure 4, P1 is the transmitted power from antenna 1 and P2 is that of antenna 2. Here, we can see STTD also retains diversity order when P2 is half of P1 (3 dB difference), and even when there is a correlation between channels and power difference. Therefore, as seen in the Figures 3 and 4, STTD is robust to spatial correlation and power imbalance. If space is limited for putting up largely separated antennas, the antenna spacing can be reduced in indoor environments where rich scattering results in low spatial correlation.

Simulations for optimizing transmitter placement were executed with respect to two performance criteria – power coverage and BER. The ray tracer's tessellation frequency was 300 for both power coverage and BER criterion. The optimizer loop takes feedback from a sophisticated wireless system model as seen in

the Figure 2. The model involves parallel 3D ray tracer and a surrogate function which estimates the BER of a WCDMA system. Two sets of simulations for optimizing transmitter placement were executed with respect to the two performance criteria – coverage and BER. Figure 5 is the floor plan of Virginia Tech Durham Hall where the calibration for the ray-tracer and the optimization for the transmitter locations optimization have been performed. Figure 6 shows that the optimizer found global optimum points based on a given criterion – BER (Bit Error Rate). The circles are three initial transmitter locations and the triangles are optimal transmitter locations based on BER criterion. The big rectangle surrounding the circles and the triangles is the area of interest we want to cover with three transmitters.

When threshold BER for optimization is set to 10^{-3}, STTD needed less transmitting power than using one antenna, as expected, covering the same area of interest with 90% meeting the threshold even though at locations where the two antennas of a transmitter are aligned each other, the diversity gain we can get from STTD degrades due to spatial correlation increase. Also, optimizing based on BER start giving different result from that of power criterion as the transmitters are loaded with more and more users. Considering interference from other transmitters, optimization of transmission power and the number of transmitters in a given indoor wireless environment add more dimensions to the optimization problem, which are not included in this study due to computational complexity.

Acknowledgement

The work in this paper was supported in part by NSF Grant #9974956.

References

[1] S.M. Alamouti, "A Simple Transmit Diversity Technique for Wireless Communications," *IEEE Journal on Selected Areas in Communications*, Vol. 16, No. 8, pp. 1451-1458, October 1998.

[2] R. Gozali and B. Woerner, "On the Robustness of Space-Time Block Codes to Spatial Correlation," *Proceedings of IEEE VTC'02, Spring*, pp. 832-836.

[3] S. Y. Seidel and T. S. Rappaport, "Site-specific Propagation Prediction for Wireless In-building Personal Communication System Design," *IEEE Transactions on Vehicular Technology*, vol. 43(4), pp. 879-891, 1994.

[4] T. S. Rappaport, *Wireless Communications: Principles and Practice*, Prentice Hall, New Jersey, 1996.

[5] A. Glassner, "Space Subdivision for Fast Ray Tracing," *IEEE Computer Graphics and Applications*, vol. 4(10), pp. 15-22, October, 1984.

[6] B. Freisleben, D. Hartmann, and T. Kielmann, "Parallel Raytracing: A Case Study on Partitioning and Scheduling on Workstation Clusters," in *Proceedings of Thirtieth International conference on System Sciences*, Hawaii, vol. 1, pp. 596-605, 1997.

[7] K. R. Schaubach, N. J. Davis IV, and T. S. Rappaport, "A Ray Tracing Method for Predicting Path Loss and Delay Spread in Microcellular Environments," in *Proceedings of IEEE VTC'92*, vol.2, pp.932-935, 1992.

[8] G. D. Durgin, T. S. Rappaport, and Hao Xu, "Measurements and Models for Radio Path Loss and Penetration Loss in and around Homes and Trees at 5.85 GHz," *IEEE Transactions on Communications*, vol. 46(11), pp.1484-1496, 1998.

[9] D. R. Jones, C. D. Perttunen, and B. E. Stuckman, "Lipschitzian Optimization without the Lipschitz Constant," *Journal of Optimization Theory and Applications*, vol. 79(1), pp. 157-181, 1993.

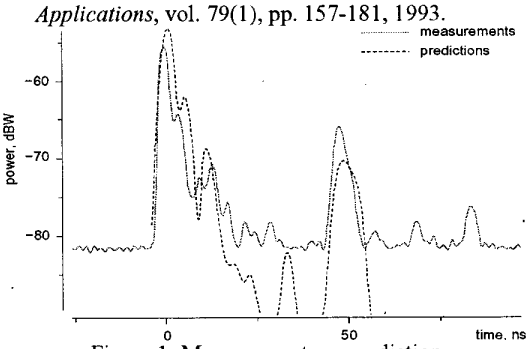

Figure 1: Measurement vs. prediction

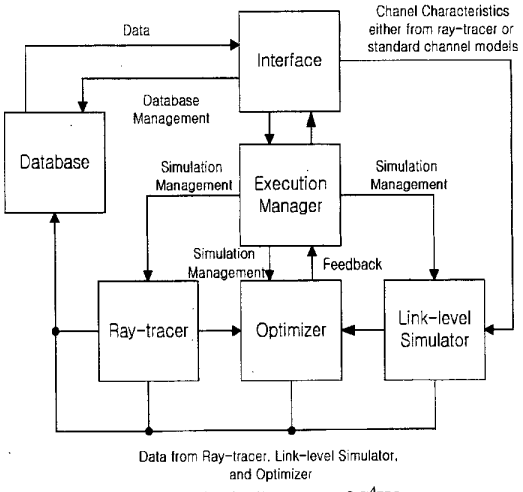

Figure 2: Block diagram of S^4W

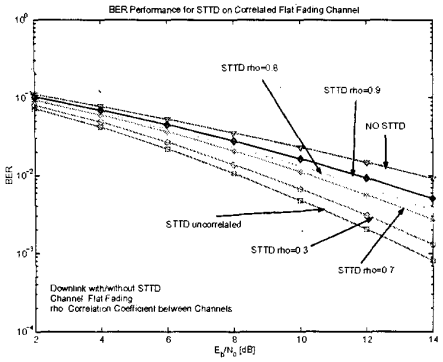

Figure 3: STTD performance on correlated channel

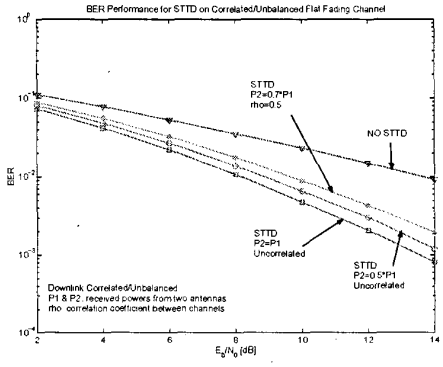

Figure 4: STTD performance on unbalanced channel

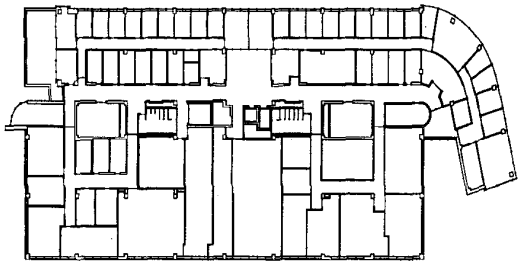

Figure 5: Durham Hall 4th floor

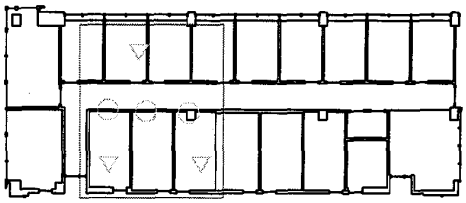

Figure 6: Optimization for three transmitter locations

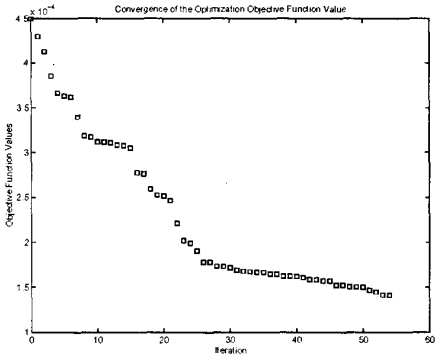

Figure 7: Convergence of the objective function value

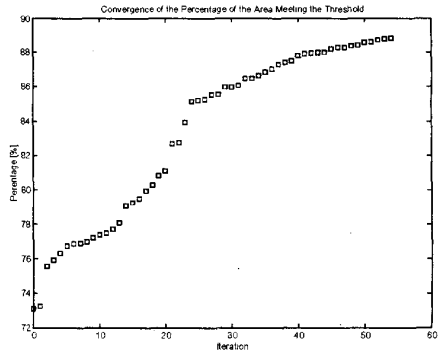

Figure 8: The percentage of the area meeting the threshold